A 3D-CNN and ICA-Guided Model for Bipolar Disorder Diagnosis via Resting-State fMRI

Noor Ayesha
CYBEX, Prince Sultan University, Riyadh, Saudi Arabia
drnayesha@gmail.com

Roaa Khalil Mohamed Ali Abed
College of Sciences and Humanities (CSH), Prince Sultan University, Riyadh, Saudi Arabia
rabed@psu.edu.sa

Saeed Ali Bahaj
MIS Department College of Business Administration, Prince Sattam Bin Abdulaziz University, Al-Kharj, Saudi Arabia
s.bahaj@psau.edu.sa (corresponding author)

Received: 10 March 2026 | Revised: 11 April 2026 | Accepted: 17 April 2026

 DOI: https://doi.org/10.48084/etasr.18633

ABSTRACT

Bipolar Disorder (BD) is a persistent mental health condition marked by intense mood fluctuations. These mood episodes range from emotional highs (mania or hypomania) to lows (depression), significantly affecting an individual's energy, activity levels, sleep patterns, behavior, and cognitive clarity. This study utilizes resting-state functional MRIs (rs-fMRI) to capture detailed structural and functional insights into brain tissue samples. Independent Component Analysis (ICA) was applied to rs-fMRI scans of 45 Healthy Controls (HCs) and 45 subjects with BD (BDs) from the OpenNeuro database to identify significant features. The top five features (IC 12, IC 15, IC 16, IC 18, and IC 22) were selected based on kurtosis, skewness, and variability, and then used as input to a 3D Convolutional Neural Network (3D-CNN) model for BD diagnosis. Of 90×5=450 independent components, the model was trained on 70% (315) and tested on the remaining 30% (135). Evaluation metrics confirmed high performance in distinguishing BD cases from HCs, achieving 94% accuracy. This approach demonstrates a reliable, high-accuracy method for diagnosing BD using rs-fMRIs, offering insights into associated functional activation patterns and neurobiological mechanisms. This multimodal approach could improve clinicians' diagnostic confidence and advance understanding of the underlying pathology of BD.

Keywords-bipolar disorder; rsfMRI; Independent Component Analysis (ICA); deep learning; health risks

I. INTRODUCTION

Bipolar Disorder (BD) is a severe chronic mental illness, also known as manic depressive disorder, characterized by significant mood swings between mania and depression. According to the Diagnostic and Statistical Manual of Mental Disorders, Fifth Edition (DSM-5), BD patients experience different problems such as increased energy, decreased need for sleep, sadness, lethargy, hopelessness, increased sexual activity, risk behavior, irritability, aggression, hyperactivity, feeling greatness, and a period of elevated mood [1]. BD occurs during adolescence or early adulthood. It is essential to recognize and optimally treat it early, as the response rate to treatment is very high in the early stages [2]. Due to its cyclic nature, it can take several months or years for an individual to be diagnosed. Due to its complexity, in the United Kingdom and the United States, on average, 10 years were estimated to be required to diagnose a patient with BD correctly [3].

MRI is a primary source for obtaining high-resolution brain images and helps to identify BD. However, in the last two decades, research has used rs-fMRI and task-related fMRI to explore the neural circuits underlying BD, with the former considered a useful scan for assessing clinical mental status, memory, and exploring the functional relationships between areas of interest in the brain [4]. This study focuses on rs-fMRI brain images of subjects suffering from BD (BDs) and Healthy Controls (HCs) for a diagnostic process using an ICA-based 3D-CNN model. ICA is a standard method for computing the clean signal from the brain, which represents the progression of neural activity over time [5]. ICA can be used to extract important features from the brains of BDs and HCs, which can be used with Machine Learning (ML) and Deep Learning (DL) models to achieve optimal accuracy. This study presents a 3D-CNN model integrated with features extracted from Independent Component Analysis (ICA) to achieve optimal accuracy. The ICA features enhance the CNN model's

performance in brain signal analysis, leading to better classification results [6]. It also provides other benefits, such as accelerating model convergence, simplifying the data, and making the training process more efficient [7].

II. LITERATURE REVIEW

Various models have been used to distinguish BDs from HCs. In [8], a Support Vector Machine (SVM) was applied to 53 HCs and 74 chronic BDs [8]. This model was applied to first-episode BD and chronic BD subjects, achieving accuracy rates of 76% and 77%, respectively. In [9], Random Forest (RF), Deep Neural Network (DNN), and Convolutional Neural Network (CNN) were applied to 32 HCs and 23 BDs using a leave-one-user-out validation strategy, with the DNN achieving 84% accuracy with SMOTE balancing. In [10], Naïve Bayes (NB), Decision Trees (DT), and K-Nearest Neighbors (KNN) were also used to assess the classification rate of BDs. The KNN model achieved 85.71% accuracy, the DT achieved 62.50% accuracy, and the NB achieved 87.50% accuracy. In [11], SVM was applied with recursive feature elimination using one-against-one and leave-one-out cross-validation methods, achieving a 70.80% accuracy. In [12], the ElasticNet model was applied to classify BDs, Major Depressive Disorder (MDD), and HCs, achieving 90% accuracy. In [13], electroencephalography data were used with an Artificial Neural Network (ANN) model to classify 31 BDs and 58 unipolar subjects, achieving an overall accuracy of 89.89% for BDs. The study in [14] employed an MRI dataset comprising 33 pediatric BD patients and 19 HCs, matched for age and gender, and six algorithms, Logistic Regression (LR), SVM, RF, NB, KNN, and AdaBoost for classification. The LR and SVM models achieved the highest accuracies, 84.19% and 82.80%, respectively, for BD classification. Similarly, fMRI and rs-fMRI datasets have been used to improve accuracy. In [15], rs-fMRI data from 48 BDs and 92 MDDs were used for classification with SVM, achieving 81% accuracy. The study in [16] used rs-fMRI data from 21 BDs, 25 MDDs, and 23 HCs for classification with an SVM-based forward-backward search strategy, achieving 92.10% accuracy. In [17], an rs-fMRI dataset of 22 BDs and 22 HCs was used for classification with an SVM, achieving an 86% accuracy. In [18], rs-fMRI data from 22 BDs, 28 MDD, and 23 HCs were used for classification with an SVM-based adaptive forward-backward greedy algorithm, achieving 88% accuracy.

This case-control study investigates an ICA-based 3D-CNN model to improve the accuracy of diagnosing BD using an rs-fMRI dataset. Previous models achieved 62–92% accuracy in classifying BD, but small datasets and limited feature extraction have limited exploration of spatiotemporal patterns. The main contributions of this study are as follows.

- The proposed model can be utilized to understand neurobiological mechanisms and brain functional activation patterns at the resting state in BDs compared to HCs.
- It also demonstrates potential in tracking oxygen levels and blood flow, allowing for observing brain activity in BD patients.
- ICA features improve the CNN model's performance in brain signal analysis, leading to faster model convergence, simplified data, increased training efficiency, and better classification results using rs-fMRIs.

III. MATERIALS AND METHODS

A. Data Acquisition and Description

The rs-fMRI dataset used to address the study aims was retrieved from the publicly available Openneuro database [19], comprising HCs and BDs. The rs-fMRI images included the following protocols: Trio Tim, EP: scanning sequence type, SK: sequence variant, Fs: scan option, MR Acquisition: 2D, epfid2d1_64: sequence name, Repetition time: 2, Echo time: 0.03, Magnetic field strength: 3T, phase encoding steps: 63, Echo train length: 1, sampling percentage: 100, phase field of view percentage: 100, pixel bandwidth: 1420, Echo planner Image factor: 128, Acceleration factor PE: 2, Aceel reference line: 24, total scan time in seconds: 312, coil name: head matrix. The device information is also as follows: device serial number: 35343, software version: syngo MR B15, protocol name: bold-resting, body: transmit coil, acquisition matrix: 64/0/0/64, COL: plane phase for encoding direction, flip angle: 90, Variable flip angle: Flag used as N, HFS, patient position, Effective echo spacing: 0.000395. 45 HCs and 45 BDs were used in this study, as shown in Table I.

TABLE I. RF-FMRI DATASET DESCRIPTION

		Age				
Group	**Gender**	**Mean**	**Max**	**Min**	**S.dev**	**Count**
BDs	Female	33.8	49.0	24.0	8.30	21
	Male	30.9	50.0	21.0	9.54	24
HCs	Female	31.7	50.0	21.0	8.89	21
	Male	32.5	49.0	21.0	9.34	24

B. Imaging Preprocessing and Denoising

The head motion was corrected across time for each subject. The realignment step corrects for subjects' head motion in the scans by aligning all volumes to a reference scan using the CONN toolbox [20, 21]:

$$x' = R(\theta_x, \theta_y, \theta_z)x + t \quad (1)$$

where R is the rotation matrix (pitch, roll, yaw), t is the translation vector (t_x, t_y, t_z), and x , x' are the original and corrected voxel coordinates. Motion correction was optimized using:

$$\min_{R,T} \sum_{v \in V} (I_t(Rx_v + t) - I_{ref}(x_v))^2 \quad (2)$$

The slice time correction is used to adjust for temporal differences arising from the sequential acquisition of slices [21], as given by:

$$y_i^{Corrected}(t_o) = y_i(t_o + \Delta_i) \quad (3)$$

where, $y_i(t)$ is the BOLD signal measured at voxel i as a function of time, t_o is the reference acquisition time, Δ_i is the time offset of slice I within a single repetition time, and $y_i^{Corrected}$ is the corrected signal at voxel i.

The human brain size varies from person to person. The following equation was used to normalize the brain scans of each subject into a standard anatomical space [21].

$$x_{MNI} = Ax_{subj} + D(x_{subj}) \quad (4)$$

where x_{subj} are the voxel coordinates in the subject's native space, x_{MNI} are the voxel coordinates in the template, A denotes translation, rotation, scaling, and shearing, and D is a nonlinear deformation field that captures complex anatomical differences not accounted for by the affine transform. The smoothing process is applied to the scans to increase the signal-to-noise ratio by averaging signals over neighboring voxels [21]. The entire smoothing process was performed using

$$y_i^{smooth} = (y * G)(x_i) = \int y(x)G(x_i - x;\sigma)dx \quad (5)$$

where $G(x;\sigma) = \frac{1}{2\pi\sigma^2}\exp\left(\frac{\|x\|^2}{2\sigma^2}\right)$ is a three-dimensional Gaussian function and σ is the full width at half maximum (FWHM)/2.355.

White matter and cerebrospinal fluid signals are considered non-neural noise and removed from the regression steps. The regression models include realignment parameters, translation and rotation, removing any type of motion signal from the BOLD [22]. Figure 1 shows detailed views of preprocessing steps, noise reduction, and BOLD % variance with a 0.25 threshold of white matter, CSF, realignment parameters, and scrubbing. All this process was done using (6-9). The confounded regression model is given by:

$$y(t) = X_c(t)\beta_c + \varepsilon(t) \quad (6)$$

where $y(t)$ is the original BOLD signal, $X_c(t)$ is the confound regressors matrix, β^c are the regression coefficients, and $\varepsilon(t)$ is the residual signal (denoised).

The confounded repressors are given by

$$X_c(t) = [W(t), C(t), M(t), S(t)] \quad (7)$$

where $W(t)$ denotes white matter signals, $C(t)$ denotes CSF signals, $M(t)$ denotes realignment parameters, and $S(t)$ denotes scrubbing regressors.

After fitting the regression model, the confounds are removed, and neural-related fluctuations are estimated using

$$s(t) = y(t) - X_c(t)\beta^c \quad (8)$$

The $s(t)$ is offering a cleaned time series containing mostly neural-related fluctuations.

The band-pass filtering process was done by using

$$s_{filtered}(t) = F^{-1}[H(f) \cdot F(s(t))] \quad (9)$$

where F denotes the Fourier transform, $H(f)$ is the frequency filter, and $s_{filtered}(t)$ is the final denoised and filtered signal.

C. Feature Selection and Proposed Predictive Model

Feature selection is important because it reduces high-dimensional input data to a lower-dimensional set of essential features. ICA is a standard way to compute the clean signal from the brain, offering brain signals as a time course to represent the progression of neural activity over time. A total of 25 components were selected for ICA for both BDs and HCs [23] using CONN. The top 5 best ICs were selected based on kurtosis, skewness, variability, and frequency for HCs and BDs because these ICs had maximum variance, meaningful signals, lower noise rate, and higher discriminative power than others. These ICs can also provide visual information on brain activation in BDs and HCs. Figure 2 shows a flowchart of the group-level ICA.

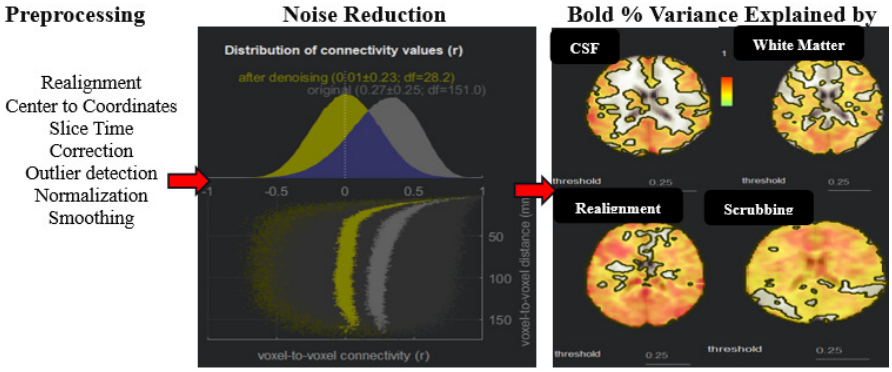

Fig. 1. Preprocessing steps, noise reduction, and BOLD % variance.

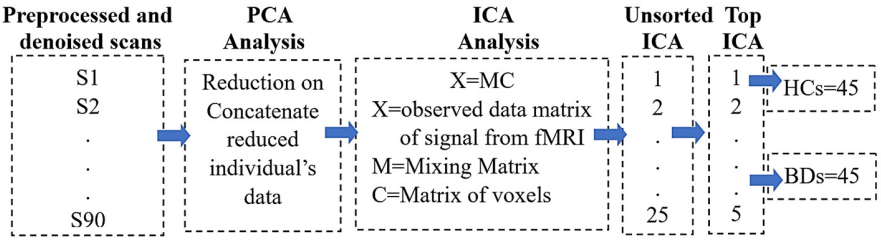

Fig. 2. Flowchart of group-level ICA of multi-subject fMRI data.

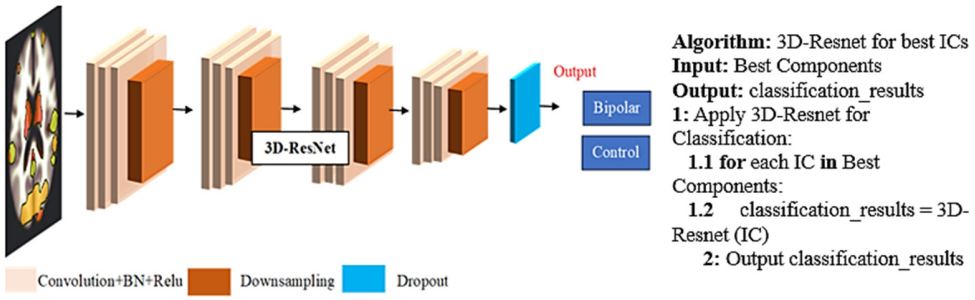

Fig. 3. Deep architecture of the proposed model.

The 3D-CNN is a DL model that can be used effectively on 3D datasets to capture patterns in the data. It has applications in various tasks such as computer vision, natural language processing, object detection, object segmentation, image classification, speech recognition, video processing, low-resolution images, resource-constrained systems, object counting, and high-dimensional datasets [24]. Due to its popularity, it is one of the most widely used DL methods. The 3D-ICs with resolution of $x = 91$, $y = 109$, $z = 91$ voxels were tuned and input to the proposed model, which has four convolutional layers, a batch normalization layer with a ReLU activation function, a down-sampling layer, and one dropout layer with a sigmoid function for the final output.

The Adaptive Moment Estimation (AdaM) optimizer was used to optimize the parameters, and binary cross-entropy was used as the loss function. A total of 25 epochs with a batch size of 5 were used to fit the model on the dataset in Google Colab using a standard GPU. Figure 3 shows a graphical view of the detailed proposed model. This study used the most dominant ICs to classify BDs from HCs using the proposed model. Out of 450 ICs, 63 subjects or 70% (315) ICs were used for training, and 27 subjects or 30% (135) were used for testing.

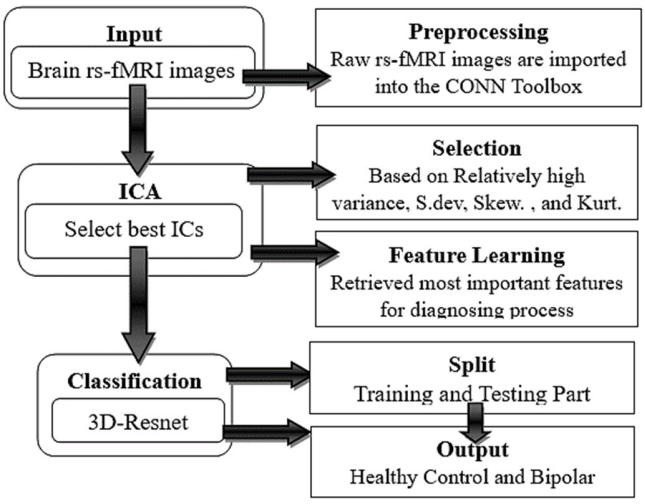

Fig. 4. Image processing mechanism of the proposed model.

D. Collaboration of 3D-CNN with ICA

The integration of ICA with the 3D-CNN provides several advantages, such as enhanced interpretability of CNN's decisions, especially in neuroimaging or financial analysis [7]. That is why the features from ICA shall be used as input features of the CNN model to distinguish BDs from HCs. The performance of the proposed model with the integration of the ICA signals was assessed using accuracy, sensitivity, specificity, False Positive Rate (FPR), False Negative Rate (FNR), confusion matrix, and ROC curve with AUC for both the training and testing datasets. Figure 4 summarizes the method followed.

IV. EXPERIMENTAL RESULTS

A. ICA for Feature Selection

ICA was used for feature extraction, identifying the most informative components from the high-dimensional raw rs-fMRI scans of both BDs and HCs. Out of 25 components, the 5 best were selected based on their kurtosis, skewness, and variability values: IC 12, IC 15, IC 16, IC 18, and IC 22. IC12 achieved kurtosis, skewness, and variability values of 19.15, 3.58, and 0.11, respectively. Similarly, IC15 showed 16.50, 3.11, 0.124; IC16, 16.16, 3.09, 0.127; IC18, 17.213, 2.908, 0.125; and IC22, 16.951, 3.328, 0.138. Based on these criteria, IC22 was selected as suitable since its spatial maps indicate noise-related patterns while preserving meaningful signals. The combination of remaining components did not improve performance, and they were excluded from the classification task. Figure 6 shows the graphical differences in the top 5 ICs between the BDs and HCs. Since it is tough to declare a person with BD based on the visual view of brain activation, there is a need for a DL model to efficiently distinguish BDs from HCs with high accuracy.

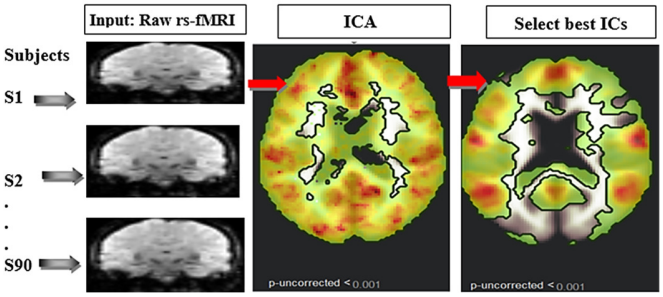

Fig. 5. Top-5 ICs from the ICA.

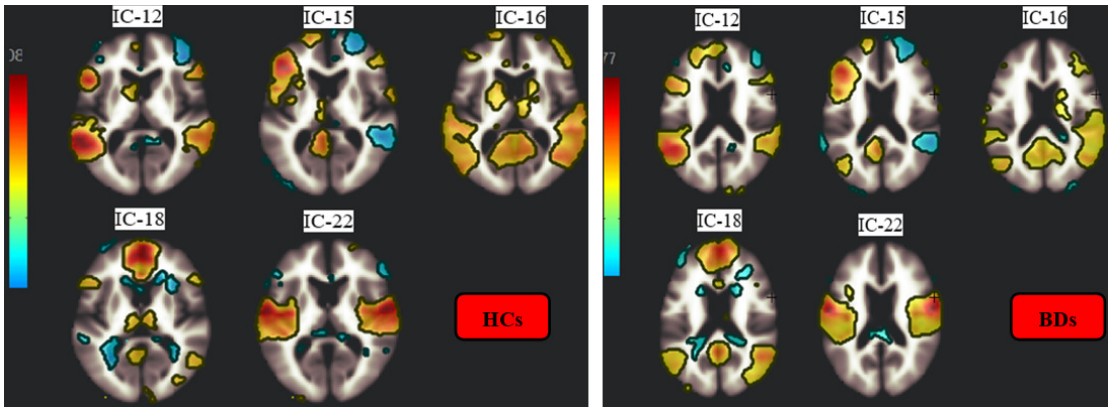

Fig. 6. Top 5 ICs of HCs and BDs, and intensity given from sky blue to red.

TABLE II. RESULTS OF ICA

ICA	Kurtosis	Skewness	Variability
1	7.90	2.175	0.113
2	9.60	2.106	0.120
3	5.92	0.79	0.13
4	6.38	0.69	0.11
5	10.3	2.43	0.10
6	7.56	1.63	0.13
7	6.40	0.81	0.10
8	6.34	0.15	0.12
9	5.41	-0.17	0.11
10	10.4	2.17	0.13
11	5.66	0.38	0.12
12	19.1	3.58	0.11
13	3.78	0.50	0.14
14	3.31	0.295	0.147
15	16.50	3.11	0.125
16	16.1	3.09	0.128
17	8.28	1.31	0.124
18	17.2	2.90	0.126
19	4.15	0.45	0.140
20	4.88	-0.97	0.134
21	11.8	2.50	0.120
22	16.9	3.32	0.138
23	3.80	0.52	0.149
24	14.7	2.68	0.119
25	6.91	1.60	0.102

B. Classification with the Proposed Model

The second aim of this study was to develop a DL model that integrates ICA to distinguish BDs from HCs. The 3D-CNN was tuned to classify the top 5 ICs for 90 subjects (45: BDs and 45: HCs). Figure 7 shows a graphical presentation of the tuning of the proposed model over 25 epochs. The proposed model based on ICA achieved 94% accuracy on both training and testing samples without under- or overfitting. The sensitivity and specificity rates were estimated at 0.94 and 0.94 for the training samples, and 0.93 and 0.95 for the testing samples, respectively. The FPR and FNR values were estimated from the training samples (0.06 each), and 0.07 and 0.06 from the testing samples. Out of 315, only 19 and 8 (3D-ICA) were incorrectly identified from the proposed model for the training and testing samples, respectively. ROC curve analysis was used to assess precision and display the discriminatory performance of the proposed model. An ROC curve value between 0.70 and 0.80 is acceptable; values above 0.80 are considered excellent, and values above 0.90 are rarely observed [25]. The proposed model achieved ROC-AUC values of 0.94 and 0.96 on the training and testing samples, as shown in Figure 8.

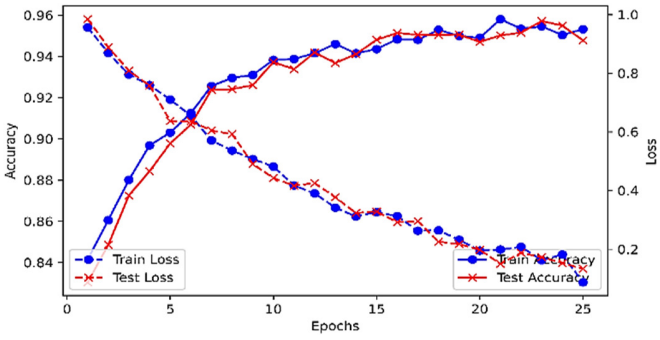

Fig. 7. Graphical presentation of the tuning proposed model.

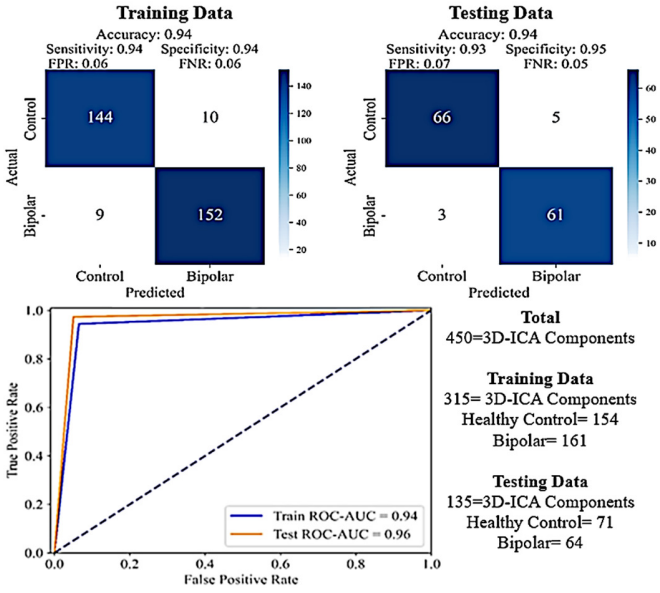

Fig. 8. Confusion matrix, classification results, and ROC curve of the proposed model.

C. Performance Metrics

Precision, recall, and F1-score were also used to evaluate the model's performance. The proposed model achieved 0.94, 0.94, and 0.94 precision, recall, and F1 scores for both the HCs and BDs, respectively, on the training samples. Similarly, on test data, the model achieved 0.96, 0.93, and 0.94 precision, recall, and F1 scores for the HC group. Similarly, on the test data, the model achieved precision, recall, and F1 scores of 0.92, 0.95, and 0.94 for the BD group. A Hosmer-Lemeshow test was performed, yielding $\chi^2 = 6.12$ with $p = 0.63$ for the training data and $\chi^2 = 4.87$ with $p = 0.77$ for the testing data, confirming good model calibration.

TABLE III. Classification report of the proposed model

	Group	Precision	Recall	f1	N	χ^2	Sig.
Train data	HCs	0.94	0.94	0.94	154	6.12	0.63
	BDs	0.94	0.94	0.94	161		
Test data	HCs	0.96	0.93	0.94	71	4.87	0.77
	BDs	0.92	0.95	0.94	64		

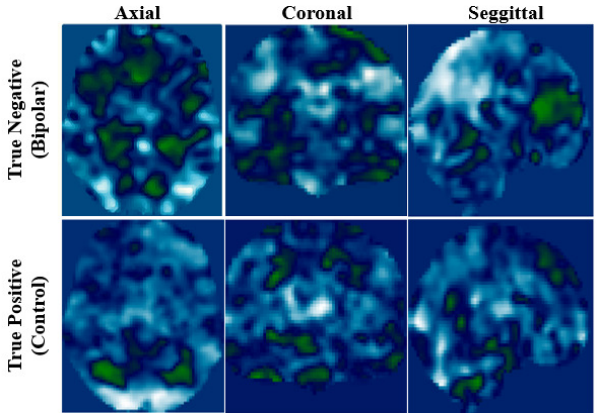

Fig. 9. Graphical activation view in the axial, coronal, and sagittal planes of TN (BD) and TP (HC) groups.

Figure 9 presents a graphical view of the TP and TN patterns of the brain's activation of HCs and BDs. The proposed model can help correctly identify 94% of a particular person who belongs to BDs or HCs.

D. Comparisons with Previous Studies

The proposed model was also compared with existing approaches that used different ML and DL approaches for BD classification, as shown in Table IV.

TABLE IV. COMPARISON WITH EXISTING STUDIES

Model	Year	Accuracy	Reference
ANN	2016	89.89%	[15]
Naïve Bayes	2016	87.50%	[11]
KNN	2016	85.17%	[11]
Decision Tree	2016	62.50%	[11]
RF and CNN	2020	84%	[10]
ElasticNet	2021	90%	[14]
SVM	2021	77%	[9]
SVM and LR	2022	84.19%	[16]
GAN-CNN	2023	75.8%	[26]
Proposed ICA+3DCNN	Present	94%	This study

E. Discussion

Physicians require a promising approach for identifying or diagnosing BDs from HCs using rs-fMRI scans. This study used the CONN toolbox for preprocessing, denoising, and ICA for BDs and HCs. ICA reduces the computational cost of the CNN model and improves prediction performance. Of 25 ICs, the 5 best were selected based on their kurtosis, skewness, and variability. IC 12, IC 15, IC 16, IC 18, and IC 22 were selected as the best components from ICA, with a high level of activation. The ICA-based 3D-CNN was used for the classification process, trained on 70% of the samples (315), tested on 30% (135), and evaluated using standard binary classification metrics. The model achieved 94% accuracy on both training and testing samples, with sensitivity and specificity rates estimated at 0.94 and 0.94 for training and 0.93 and 0.95 for testing samples. The proposed model also achieved low FPR and FNR for training and testing datasets. Out of 315, only 19 and 8 components were incorrectly identified in training and testing, respectively. ROC-AUC values of 0.94 and 0.96 were achieved on training and testing, respectively, indicating strong discriminatory power. In addition, a comparison with previous studies showed that the proposed model achieved higher accuracy.

In summary, this study is an essential step toward clinically diagnosing BDs from HCs, demonstrating that ICA can be utilized to understand the neurobiological mechanisms and functional activation patterns in the resting state of BDs and HCs. These findings can help physicians and researchers track oxygen levels and blood flow to observe brain activity in BD patients. ICA analysis also facilitates understanding of brain activation conditions and the diagnosis of BDs compared with HCs, while its integration with a 3D CNN can lead to better classification results.

V. CONCLUSION

This research presented a promising approach with a high confidence level for diagnosing BDs from HCs using rs-fMRI scans. The IC 12, IC 15, IC 16, IC 18, and IC 22 were selected as the best components from the ICA and used as input to the 3D-CNN model to identify HCs and BDs. The strength of the proposed model was validated by large values in accuracy, sensitivity, specificity, precision, recall, F1-score, and ROC-AUC, and smaller values of FPR and FNR, outperforming existing models. The findings of this study can help physicians and researchers track oxygen levels, neurobiological mechanisms, and functional activation patterns, and increase confidence in declaring an individual a BD patient. However, this study is limited by dataset size and lack of external validation. Future work will focus on larger, multi-site datasets and extending the model to multi-class classification (e.g., BDs vs. MDD vs. HCs) to enhance generalizability and clinical applicability.

ACKNOWLEDGMENT

The authors would like to acknowledge the support of Prince Sultan University, Riyadh, Saudi Arabia, for APC support for this publication.

CONFLICTS OF INTEREST

The authors declare no conflicts of interest in this work.

DATA AVAILABILITY

The data that support the findings of this study are available in [19].

REFERENCES

[1] S. Z. Kurdi, "Machine Learning–Based Classification Framework for Human Health Care Monitoring," *International Journal of Theoretical & Applied Computational Intelligence*, vol. 2026, pp. 1–15, Jan. 2026, https://doi.org/10.65278/IJTACI.2026.1.

[2] M. S. Shobini and M. Sudha, "BiPoP: Bipolar Disorder Optimized Preprocessing Framework for Stress Disorder Identification through Gene Expression Data using Deep Learning," *Engineering, Technology & Applied Science Research*, vol. 15, no. 2, pp. 22126–22130, Apr. 2025, https://doi.org/10.48084/etasr.9776.

[3] T. Saba, A. Rehman, M. N. Shahzad, R. Latif, S. A. Bahaj, and J. Alyami, "Machine learning for post-traumatic stress disorder identification utilizing resting-state functional magnetic resonance imaging," *Microscopy Research and Technique*, vol. 85, no. 6, pp. 2083–2094, 2022, https://doi.org/10.1002/jemt.24065.

[4] H. Ali, "A Meta-Review of Computational Intelligence Techniques for Early Autism Disorder Diagnosis," *International Journal of Theoritical & Applied Computational Intelligence*, pp. 01–21, 2025, https://doi.org/10.65278/IJTACI.2025.1.

[5] H. K. Aljobouri, "Independent Component Analysis with Functional Neuroscience Data Analysis," *Journal of Biomedical Physics and Engineering*, vol. 13, no. 2, Apr. 2023, https://doi.org/10.31661/jbpe.v0i0.2111-1436.

[6] A. Y. Abdzaid, D. N. Khadum, S. S. Al-Barrak, and A. Saad, "White Blood Cells Classification Based on a New Strategy to Cluster Channels RGB of Blood Smear Image Using Resnet-18 Model," *International Journal of Theoretical & Applied Computational Intelligence*, vol. 2026, pp. 120–131, Apr. 2026, https://doi.org/10.65278/IJTACI.2026.64.

[7] B. Shehu Aliyu, J. Isuwa, A. Abdulrahim, M. Abdullahi, I. Hayatu Hassan, and T. Sikder Momi, "Enhanced Feature Selection for Imbalanced Microarray Cancer Gene Classification Using Chaotic Salp Swarm Algorithm," *International Journal of Theoritical & Applied Computational Intelligence*, pp. 259–283, 2025, https://doi.org/10.65278/IJTACI.2025.16.

[8] J. Sawalha *et al.*, "Individualized identification of first-episode bipolar disorder using machine learning and cognitive tests," *Journal of Affective Disorders*, vol. 282, pp. 662–668, Mar. 2021, https://doi.org/10.1016/j.jad.2020.12.046.

[9] P. Jakobsen *et al.*, "Applying machine learning in motor activity time series of depressed bipolar and unipolar patients compared to healthy controls," *PLOS ONE*, vol. 15, no. 8, Aug. 2020, Art. no. e0231995, https://doi.org/10.1371/journal.pone.0231995.

[10] C. Saylan and K. Yilancioglu, "Classification of schizophrenia and bipolar disorder by using machine learning algorithms," *The Journal of Neurobehavioral Sciences*, vol. 3, no. 3, pp. 92–95, 2016.

[11] M. Chen *et al.*, "Distinguishing schizophrenia and bipolar disorder through a Multiclass Classification model based on multimodal neuroimaging data," *Journal of Psychiatric Research*, vol. 172, pp. 119–128, Apr. 2024, https://doi.org/10.1016/j.jpsychires.2024.02.024.

[12] S. Poletti *et al.*, "A peripheral inflammatory signature discriminates bipolar from unipolar depression: A machine learning approach," *Progress in Neuro-Psychopharmacology and Biological Psychiatry*, vol. 105, Mar. 2021, Art. no. 110136, https://doi.org/10.1016/j.pnpbp.2020.110136.

[13] Turker Tekin Erguzel, Gokben Hizli Sayar, and N. Tarhan, "Artificial Intelligence Approach to Classify Unipolar and Bipolar Depressive Disorders." ResearchGate, 2015, https://doi.org/10.13140/RG.2.1.3168.5284.

[14] R. Dou *et al.*, "Machine learning algorithm performance evaluation in structural magnetic resonance imaging-based classification of pediatric bipolar disorders type I patients," *Frontiers in Computational Neuroscience*, vol. 16, Aug. 2022, Art. no. 915477, https://doi.org/10.3389/fncom.2022.915477.

[15] X. Jiang *et al.*, "Identifying misdiagnosed bipolar disorder using support vector machine: feature selection based on fMRI of follow-up confirmed affective disorders," *Translational Psychiatry*, vol. 14, no. 1, Jan. 2024, Art. no. 9, https://doi.org/10.1038/s41398-023-02703-z.

[16] N. F. Jie *et al.*, "Discriminating Bipolar Disorder From Major Depression Based on SVM-FoBa: Efficient Feature Selection With Multimodal Brain Imaging Data," *IEEE Transactions on Autonomous Mental Development*, vol. 7, no. 4, pp. 320–331, Sept. 2015, https://doi.org/10.1109/TAMD.2015.2440298.

[17] M. Li *et al.*, "Clinical utility of a short resting-state MRI scan in differentiating bipolar from unipolar depression," *Acta Psychiatrica Scandinavica*, vol. 136, no. 3, pp. 288–299, Sept. 2017, https://doi.org/10.1111/acps.12752.

[18] N. F. Jie *et al.*, "Discriminating Bipolar Disorder from Major Depression using Whole-Brain Functional Connectivity: a Feature Selection Analysis with SVM-FoBa Algorithm," *Journal of Signal Processing Systems*, vol. 90, no. 2, pp. 259–271, Feb. 2018, https://doi.org/10.1007/s11265-016-1159-9.

[19] R. Bilder *et al.*, "UCLA Consortium for Neuropsychiatric Phenomics LA5c Study." Openneuro, 2020, https://doi.org/10.18112/OPENNEURO.DS000030.V1.0.0.

[20] "CONN toolbox." https://web.conn-toolbox.org/.

[21] H. A. Jaber, H. K. Aljobouri, İ. Çankaya, O. M. Koçak, and O. Algin, "Preparing fMRI Data for Postprocessing: Conversion Modalities, Preprocessing Pipeline, and Parametric and Nonparametric Approaches," *IEEE Access*, vol. 7, pp. 122864–122877, 2019, https://doi.org/10.1109/ACCESS.2019.2937482.

[22] Y. Behzadi, K. Restom, J. Liau, and T. T. Liu, "A component based noise correction method (CompCor) for BOLD and perfusion based fMRI," *NeuroImage*, vol. 37, no. 1, pp. 90–101, Aug. 2007, https://doi.org/10.1016/j.neuroimage.2007.04.042.

[23] M. N. Shahzad and H. Ali, "Deep learning based diagnosis of PTSD using 3D-CNN and resting-state fMRI data," *Psychiatry Research: Neuroimaging*, vol. 343, Sept. 2024, Art. no. 111845, https://doi.org/10.1016/j.pscychresns.2024.111845.

[24] S. Nasir, M. Bilal, and H. Khalidi, "Detection and Classification of Skin Cancer by using CNN-Enabled Cloud Storage Data Access Control Algorithm based on Blockchain Technology," *International Journal of Theoritical & Applied Computational Intelligence*, pp. 146–159, 2025, https://doi.org/10.65278/IJTACI.2025.31.

[25] M. N. Shahzad, H. Ali, T. Saba, A. Rehman, H. Kolivand, and S. A. Bahaj, "Identifying Patients With PTSD Utilizing Resting-State fMRI Data and Neural Network Approach," *IEEE Access*, vol. 9, pp. 107941–107954, 2021, https://doi.org/10.1109/ACCESS.2021.3098453.

[26] M. H. Saghayan, M. H. Zolfagharnasab, A. Khadem, F. Matinfar, and H. Rashidi, "Diagnosing Bipolar Disorder from 3-D Structural Magnetic Resonance Images Using a Hybrid GAN-CNN Method." arXiv, 2023, https://doi.org/10.48550/ARXIV.2310.07359.